Quantitative phosphoproteomic analysis of acquired cancer drug resistance to pazopanib and dasatinib

Simon Vyse[1*], Frank McCarthy[1*], Malgorzata Broncel[1*#], Angela Paul[2], Jocelyn P Wong[1], Amandeep Bhamra[2] and Paul H Huang[1,3].

Affiliations:

[1]Division of Cancer Biology and [2]Proteomics Core Facility, The Institute of Cancer Research, London, SW3 6JB, UK.

*These authors contributed equally to this work.

[#]Current address: The Francis Crick Institute, 1 Midland Road, London NW1 1AT, UK.

[3]Correspondence:

Paul H Huang
Division of Cancer Biology
The Institute of Cancer Research
London SW3 6JB
United Kingdom
Email: paul.huang@icr.ac.uk
Tel: +44 207 153 5554

Running title: Phosphoproteomics of pazopanib and dasatinib resistance.

Keywords: Phosphoproteomics, kinase inhibitors, drug resistance, pazopanib, dasatinib, cell signalling

Abstract

Acquired drug resistance impacts the majority of patients being treated with tyrosine kinase inhibitors (TKIs) and remains a key challenge in modern anti-cancer therapy. The lack of clinically effective therapies to overcome resistance represents an unmet need. Understanding the signalling that drives drug resistance will facilitate the development of new salvage therapies to treat patients with secondary TKI resistance. In this study, we utilise mass spectrometry to characterise the global phosphoproteomic alterations that accompany the acquisition of resistance to two FDA-approved TKIs, pazopanib and dasatinib, in the A204 rhabdoid tumour cell line. Our analysis finds that only 6% and 9.7% of the quantified phosphoproteome is altered upon the acquisition of pazopanib and dasatinib resistance respectively. Pazopanib resistant cells display elevated phosphorylation in cytoskeletal regulatory pathways while dasatinib resistant cells show an upregulation of the insulin receptor/IGF-1R signalling pathway. Drug response profiling rediscovers several previously reported vulnerabilities associated with pazopanib and dasatinib resistance and identifies a new dependency to the second generation HSP90 inhibitor NVP-AUY-922. This study provides a useful resource detailing the candidate signalling determinants of acquired TKI resistance; and reveals a therapeutic approach of inhibiting HSP90 function as a means of salvage therapy to overcome pazopanib and dasatinib resistance.

Significance

Pazopanib and dasatinib are tyrosine kinase inhibitors (TKIs) approved for the treatment of multiple cancer types. Patients who are treated with these drugs are prone to the development of drug resistance and consequently tumour relapse. Here we use quantitative phosphoproteomics to characterise the signalling pathways which are enriched in cells that have acquired resistance to these two drugs. Furthermore, targeted drug screens were used to identify salvage therapies capable of overcoming pazopanib and dasatinib resistance. This data advances our understanding of the mechanisms of TKI resistance and highlights candidate targets for cancer therapy.

Introduction

Tyrosine kinase inhibitors (TKIs) have emerged as a major class of anti-cancer agents that display efficacy in a range of tumour types including lung cancer, chronic myeloid leukaemia (CML) and gastrointestinal stromal tumours (GIST) [1, 2]. However efficacy is often short-lived with the majority of patients going on to develop acquired resistance and tumour recurrence after prolonged drug treatment [3]. Studies in cell line models have revealed several major mechanisms of resistance that have been clinically observed, including the acquisition of drug resistant mutations in the target kinase, activation of bypass signalling pathways and phenotypic alterations such as epithelial-mesenchymal-transition (EMT) [3-6]. These drug resistant cells arise either from selection of pre-existing clones within a heterogeneous tumour cell population or through the adaptation and subsequent evolution of drug-tolerant persister cells [7, 8]. Given that most patients who progress on TKI treatment have limited options for subsequent lines of therapy, there is an urgent need to develop effective salvage therapies to treat patients whose tumours relapse as a result of acquired drug resistance.

Pazopanib and dasatinib are multi-target TKIs that inhibit a distinct but overlapping spectrum of tyrosine kinases [9-12]. Pazopanib is approved for advanced soft tissue sarcoma and

renal-cell carcinoma [13, 14] while dasatinib is licensed for the treatment of CML and Philadelphia chromosome-positive acute lymphoblastic leukaemia (ALL) [15, 16]. Of note, the mechanisms of acquired resistance to pazopanib are poorly characterised in part because there are very few cell line models that harbour intrinsic sensitivity to this drug [17]. Despite the largely distinct target selectivity profiles of these two drugs, we have recently demonstrated that in the context of the SMARCB1-deficient rhabdoid tumour cell line A204, acquired resistance to these two compounds is associated with the downregulation of a common target PDGFRα [12]. This acquired resistance could be overcome by the inhibition of bypass signalling initiated by the FGFR1 kinase with inhibitors such as BGJ398, AZD4547 and ponatinib as salvage therapy [12].

Although our laboratory was able to identify common molecular alterations in PDGFRα and FGFR1 in the dasatinib- and pazopanib-resistant A204 cell lines, gene expression and copy number analyses of these cells have revealed clear differences between their molecular profiles [12]. For instance, the dasatinib-resistant cells harboured additional gains on chromosome 17 and losses in chromosome 13 which were not observed in the pazopanib-resistant line [12]. These differences suggest that there are likely to be additional dependencies associated with acquired resistance to dasatinib and pazopanib which can be exploited for cancer therapy. Furthermore, the phosphotyrosine (pTyr)-based proteomics employed in our previous study was only able to identify <5 tyrosine phosphorylated proteins that were upregulated in the two TKI resistant cell lines [12], limiting our ability to determine the signalling pathways enriched as a result of acquired drug resistance. The lack of significantly upregulated pTyr-containing proteins raises the possibility that the major alterations associated with drug resistance in the A204 cells may instead be driven by phosphoserine (pSer) and phosphothreonine (pThr) signalling events.

In this study we employ a global phosphoproteomics analysis strategy to identify pSer/pThr signalling alterations enriched in the pazopanib- (PazR) and dasatinib-resistant (DasR) A204

cell lines. In addition, we perform a targeted drug profiling analysis to determine new vulnerabilities associated with pazopanib and dasatinib resistance in these cells; with the goal of identifying additional salvage therapy candidates to treat patients who have acquired resistance to these drugs. Phosphoproteomics has been extensively used to reveal signalling pathways driving resistance to multiple TKIs including the approved drugs erlotinib, lapatinib, imatinib and sorafenib among others [18-23]. More recently, the value of utilising small panels of targeted drugs directed against key regulators of cancer cell survival to screen for combinations to overcome acquired drug resistance has been successfully demonstrated in lung cancer [24]. Here we utilise these two approaches to determine the signalling pathways which are enriched in pazopanib- and dasatinib-resistant cells and uncover a new vulnerability to the HSP90 inhibitor NVP-AUY-922 which has utility in overcoming acquired resistance to these TKIs.

Methods

Cell culture and derivation of acquired resistant sublines

Cells were cultured in DMEM media supplemented with 10% FBS, 2mM glutamine, 100units/ml penicillin and 100mg/ml streptomycin in 95% air, 5% CO2 atmosphere at 37°C. For SILAC experiments, A204 cells and resistant sublines were cultured in SILAC DMEM media (Thermo Fisher Scientific) supplemented with light lysine and arginine (R0K0) (Sigma) and heavy lysine and arginine (R10K8) (Goss Scientific), respectively. To generate resistant sublines, A204 cells were grown initially in DMEM media containing Dasatinib and Pazopanib (LC laboratories) at a concentration of 500nM [12]. The drug was incremented when the cells had proliferated to near confluency alongside minimal visible cell death. Drug concentration was incremented from 2μM to 3μM and 5μM in a stepwise manner over 6 weeks. A final drug concentration of 5μM was maintained in resistant cells. Media and drug were replenished twice weekly.

Cell Viability Assays

Cells (2,000/well) were seeded in a 96-well plate and treated with inhibitors at the indicated drugs and doses for 72 hr prior to assessment of cell viability using Cell Titre Glo (Promega), following the manufacturer's recommendations. IC_{50} data were generated from dose-response curves fitted using a four-parameter regression fit in GraphPad Prism 6 software. Inhibitors used in this study include Gefitinib, Rociletinib, Lapatinib, Neratinib, Sorafenib, Ceritinib, Crizotinib, Pazopanib, Sunitinib, Dasatinib, Ponatinib, AZD4547, Bosutinib, BEZ235, Trametinib, NVP-AUY-922, Imatinib (LC laboratories) AZD9291, PF-562271, Palbociclib, BGJ398, MK2206, AZD5363 (Selleck Chemicals), BX-795, MRT67307 (Sigma-Aldrich), JQ1 (Cayman Chemical Company), DDR1-in-1 (Tocris), CCT244747 (ICR).

Colony formation assays

Cells were seeded at low density (10,000 / well) in 6 well plates and after 24h were treated with inhibitors at the indicated doses for a duration of 2 weeks. Media containing inhibitors was replenished every 72h. Following this, cells were fixed using Carnoy's Fixative (3:1 methanol: acetic acid) and stained with 1% crystal violet solution (Sigma-Aldrich).

Phosphoproteomic enrichment and sample preparation

Phosphoproteomic analysis was performed as previously described [25] with the following modifications: SILAC labelled cells (biological triplicates) were lysed in 8M urea and equal amounts of heavy (DasR or PasR cells) and light (parental cells) lysates were mixed prior to reduction, alkylation and trypsin digestion. Peptides were desalted on a C18 cartridge, eluted with 25% acetonitrile and lyophilised to dryness. The sample was reconstituted with 400 µl of IP buffer (100 mM Tris, 100 mM NaCl, 0.3% NP-40, pH 7.4) and the pH was adjusted to 7.4. After immuno-precipitation with pTyr100, pTyr1000 (Cell Signaling Technology) and 4G10 (Merck Millipore) for the phosphotyrosine-containing peptides, which were used in a prior study [12], the supernatant was subjected to phosphopeptide enrichment. 2 mg of cell lysate

from the supernatant was enriched for phosphopeptides using sequential immobilized metal affinity chromatography (IMAC) on $FeCl_3$ charged NTA beads as previously described [25].

A further 2 mg of cell lysate from the supernatant was separately enriched for phosphopeptides using TitanSphere Phos-TiO_2 spin tips (GL Sciences). Spin tips were conditioned using 2 x 20 μl 80% acetonitrile/0.4% trifluoroacetic acid solution, followed by equilibration at with 20 μl 60% acetonitrile/0.3% trifluoroacetic acid/25% lactic acid. Tips were spun at 3000 x g for 2 minutes between each conditioning or equilibration step. The starting peptide sample was vacuum dried and reconstituted in 50 μl 0.1% trifluoroacetic acid solution. The reconstituted sample was mixed with 150 μl 60% acetonitrile/0.3% trifluoroacetic acid/25% lactic acid, added to an equilibrated spin tip and spun at 1000 x g for 10 mins. The flow through was collected and applied an additional two more times to the same spin tip to enhance adsorption of phosphopeptides. Following this, the flow through was then applied to a new spin tip and the same enrichment process was followed and analysed separately. After binding of phosphopeptides, spin tips were rinsed twice with 20 μl 60% acetonitrile/0.3% trifluoroacetic acid/lactic acid and five times with 20 μl of 80% acetonitrile/0.4% trifluoroacetic acid and spun at 3000 x g for 2 minutes between each step. Phosphopeptides were eluted using 2 x 50 μl of 5% NH_4OH solution and 1 x 50 μl pyrrolidine. Eluates were combined and vacuum dried before LC-MS/MS analysis.

Liquid Chromatography-Tandem Mass Spectrometry (LC-MS/MS)

For IMAC-enriched samples, reversed phase chromatography was performed on eluted peptides using a Dionex UltiMate 3000 RSLC nano system (Thermo Fisher Scientific). The phosphopeptide-enriched eluates were analysed as 6 μL injections, and loaded on to a Acclaim PepMap100 C18 trap cartridge trap cartridge at 8 μL/min 2% acetonitrile/0.1% trifluoroacetic acid (0.5 mm i.d. x 5 mm, 5 μm bead size, 100 Å pore size; loaded in a bi-directional manner). Peptides were then resolved on a 75 μm I.D. 15 cm C18 packed emitter

column (3 µm particle size; NIKKYO TECHNOS CO.,LTD). Phosphopeptide-enriched samples were run over 125 min using a three-step gradient of 96:4 to 65:35 buffer A:B (t = 0 min 4% B, 5 min 4% B, 14 min 10% B, 118 min 35% B, 125 min 50% B) at 250 nL/min. Peptides were ionised by electrospray ionisation using 1.8 kV applied immediately pre-column via a microtee built into the nanospray source. Sample was infused into an LTQ Velos Orbitrap mass spectrometer (Thermo Fisher Scientific) directly from the end of the tapered tip silica column (6-8 µm exit bore). The ion transfer tube was heated to 275°C and the S-lens set to 60%. MS/MS were acquired using data dependent acquisition based on a full 30,000 resolution FT-MS scan with preview mode disabled and no internal lock mass was used. The top 10 most intense ions were fragmented using enhanced ion trap scans. Precursor ions with unknown or single charge states were excluded from selection. Automatic gain control was set to 1,000,000 for FT-MS and 30,000 for IT-MS/MS, full FT-MS maximum inject time was 500 ms and normalised collision energy was set to 35% with an activation time of 10 ms. Total lysate peptides were subjected to wideband activation to co-fragment precursor ions undergoing neutral loss of up to -20 m/z from the parent ion, including loss of water/ammonia. Multistage activation (MSA) was used to target phosphoserine/threonine peptides by fragmenting precursor ions undergoing neutral loss of 32.70, 49.00, 65.40 and 98.00 m/z, corresponding to neutral loss of phosphate, if observed in the top 3 most intense fragment ions. MS/MS was acquired for selected precursor ions with a single repeat count acquired after 8 s delay followed by dynamic exclusion with a 10 ppm mass window for 45 s based on a maximal exclusion list of 500 entries.

The equivalent of 2 µg of total lysate was also run according to the above conditions to measure the total proteome for subsequent normalisation of phosphoproteomic data. The total lysates were run over 245 min using a three-step gradient of 96:4 to 65:35 buffer A:B (t = 0 min 4% B, 5 min 4% B, 45.0 min 10% B, 230.0 min 35% B, 245.0 min 50% B) and the top 20 most intense ions were fragmented by collision-induced dissociation and analysed using normal ion trap scans as described above.

For TiO_2-enriched samples, peptides were resolved on a 75 µm I.D. 50 cm C18 Easy-Spray packed emitter column (2 µm particle size; PepMap RSLC, Thermo Fisher Scientific) over 240 min using a multi-step gradient of buffers A:B (t=0 min 5% B, t=5.5 min 4% B, t= 45 min 10% B, t = 175 min 25% B, t = 245 min 50% B, t= 250 min, 95% B, t= 255 min, 95% B, t = 260 min 4% B, t= 280 4% B) (buffer A: 2% acetonitrile/0.1% formic acid; buffer B: 80% acetonitrile/0.1% formic acid) at 250 nL/min. Peptides were ionised by electrospray ionisation using 2.3 kV applied using the Easy-Spray ion Source. Sample was infused into a Q-Exactive HF mass spectrometer (Thermo Fisher Scientific) directly from the packed emitter (5 µm exit bore). The ion transfer tube was heated to 275°C and the S-lens set to 50%. MS/MS were acquired using data dependent acquisition based on a full FT-MS scan from 350 to 1850 m/z at 120,000 resolution, with a target Automatic Gain Control (AGC) value of 3,000,000 and a maximum injection time of 50 ms. No internal lock mass calibrant was used. The top 15 most intense ions were fragmented by higher energy collision-induced dissociation (HCD) and dynamically excluded for 30 s. The normalised collision energy was set to 32 with an activation time of 10 ms. Precursor ions with unknown or single charge states were excluded from selection. Fragmented ions were scanned in the FT-Orbitrap at 60,000 resolution (selected first mass at 100 m/z) with a target AGC value of 50,000 and a maximum injection time of 100 ms.

Data analysis

The data were processed with MaxQuant [26] (version 1.5.5.1) and the peptides were identified (maximal mass error = 6 ppm and 20 ppm for precursor and product ions, respectively) from the MS/MS spectra searched against human UniProt database using Andromeda [27] search engine. The following peptide bond cleavages: arginine or lysine followed by any amino acid (a general setting referred to as Trypsin/P) and up to two missed cleavages were allowed. SILAC based experiments in MaxQuant were performed using the built-in quantification algorithm [26] with minimal ratio count = 2 and enabled ‘Requantify’ feature. For each of the three biological replicate experiments, two technical replicates of the

IMAC-phosphopeptide enrichment; two technical replicates of the TiO_2-phosphopeptide enriched samples; and three technical replicates of the total proteome were analysed. Cysteine carbamidomethylation was selected as a fixed modification whereas methionine oxidation; deamidation of asparagine and glutamine; glutamine to pyro-glutamic acid; acetylation of protein N-terminus; with phospho (STY) as variable modifications for phosphoproteome searches. The false discovery rate was set to 0.01 for peptides, proteins and sites. Other parameters were used as default in the software. "Unique and razor peptides" mode was selected to allow identification and quantification of proteins in groups. Data were further analysed using Microsoft Office Excel 2010 and Perseus [28] (version 1.5.5.3). Both phosphoproteomic and proteomic data were filtered to remove potential contaminants and IDs originating from reverse decoy sequences. Proteomic data was also filtered to exclude proteins only identified by site. To account for deviations from a 1:1 mix of heavy:light starting material, the median H/L ratio across the entire proteome dataset was used to normalize the phosphoproteomic dataset. The $\log_2$ values of the H/L ratios were then determined. Phosphorylation sites (STY) were filtered to include only high confidence phosphosite IDs (localization probability ≥ 75%). The dataset was then filtered for only valid quantifiable IDs in at least two out of three biological replicates. The mass spectrometry proteomics data have been deposited to the ProteomeXchange Consortium via the PRIDE [29] partner repository with the dataset identifier PXD005536.

Bioinformatic analysis

Biological replicate overlap and phosphorylated amino acid distribution were analysed within Perseus (1.5.5.1) [28]. The phosphoproteome dataset was then annotated with the PhosphositePlus known sites database [30]. The online tool Venny 2.1 (http://bioinfogp.cnb.csic.es/tools/venny/) was used to generate Venn diagrams and GraphPad Prism 7.02 was used to generate the pie charts.

One sample t-tests were performed on SILAC $\log_2$ ratios to determine significantly different regulated phosphosites; where the null hypothesis was that the phosphopeptide abundances were unchanges and the Log2 SILAC ratio was equal to 0. Those phosphosites that were either two-times up-regulated in the A204 parental (t-test difference < -1) or up-regulated in the PazR or DasR (t-test difference > 1) cells and significantly different ($p < 0.05$) were analysed for enrichment. These data are presented as volcano plots generated in GraphPad Prism 7.02 where the statistical significance ($p < 0.05$) was $-\log_{10}$ transformed (y-axis) and plotted against the t-test difference (x-axis).

Enrichment analysis was performed using DAVID Bioinformatics Resources 6.8 [31] with human genome as a background dataset. KEGG (Kyoto encyclopedia of genes and genomes) [32], Uniprot keyword and sequence feature categories [33], Interpro protein function analysis [34], SMART (Simple Modular Architecture Research Tool) protein domain [35] and COG (Clusters of Orthologous Groups) Analysis Ontology [36] annotation databases were used for analysis. Protein annotation enrichment analysis of the phosphoproteome dataset was performed using the DAVID functional annotation tool and a modified Fisher Exact Test called EASE (Expression Analysis Systematic Explorer) score, comparing up-regulated phosphorylated proteins of PazR and DasR with their corresponding up-regulated phosphorylated proteins in the A204 parental cell line. A statistical cut off of 0.005 was applied. Multiple hypothesis testing was controlled using a Benjamini-Hochberg FDR threshold of 0.1. An intersection size of 3 or more was considered to be enriched. A bar chart of the data was then generated within GraphPad Prism 7.02. Additionally, the DAVID enrichment analysis was subjected to network mapping for visualisation using the application EnrichmentMap 2.2.1 within the Cytoscape 3.4.0 software [37]. Lists of phosphoproteins from enrichment clusters were generated and further investigated using the online application STRING 10.5 [38] to construct protein networks and analyse their associations. If necessary, 5 additional STRING interactors were imputed to the networks to propose

possible intact, but not measured, systems. The network images were generated from the STRING output of proteins and their interaction score using Cytoscape 3.4.0.

For drug screen analysis, clustering was performed and heat maps generated within Perseus as described above across each dose of drug (100 or 500 nM) and cell line (A204 parental, DasR and PazR) using cell viability values normalised to DMSO control (n=2 or 3).

Results

Characterisation of the phosphoproteome in parental and acquired resistant A204 cells

Pazopanib resistant (PazR) and dasatinib resistant cells (DasR) were previously derived from the A204 parental cell line by long-term escalating dose treatment with drug [12] (Figure 1A). Briefly, A204 cells were initially grown in media containing 500nM of pazopanib or dasatinib and the drug dose increased when the cells proliferated to near confluency alongside minimal visible cell death. Drug concentration was then increased from 2μM to 3μM and then 5μM in a stepwise manner over 6 weeks. A final drug concentration of 5μM was maintained in resistant cells. We subjected the cell lines to stable isotope labelling with amino acids in cell culture (SILAC) with the PazR and DasR cells being 'heavy labelled' and the parental A204 cell line being 'light labelled' (Figure 1A). Cells were lysed, combined in a 1:1 ratio and lysates digested with trypsin. We have performed an analysis of the pTyr phosphoproteome of these cells using phosphopeptide immunoprecipitation of the SILAC labelled cell lysates in a previously reported study [12]. In this current study, the supernatant from this pTyr immunoprecipitation was subjected to either immobilised metal affinity chromatography (IMAC) or titanium dioxide (TiO_2) phosphopeptide enrichment prior to single-shot liquid chromatography tandem mass spectrometry (LC-MS/MS) in biological triplicates (Figure 1B). The mass spectrometry data from both phosphopeptide enrichment strategies were combined and analysed together using the MaxQuant algorithm [26]

Collectively, we identified 7214 unique phosphorylation sites on 2372 proteins in the PazR/A204 comparison and 7548 unique phosphosites on 2494 proteins in the DasR/A204 comparison across all three biological replicates (Figure 1C and Table S1 and S2). In both sets of experiments, analysis of the distribution of phosphorylated residues shows the expected classical distribution of pSer:pThr:pTyr ratios (~90:10:1) as previously reported (Figure S1A) [39]. We observed pTyr sites (~1% of all phosphosites) in the analysis despite prior pTyr phosphopeptide enrichment (Figure S1A), indicating that immunoprecipitation did not deplete all the pTyr-containing peptides in the lysate. This may be the result of previously reported restricted pTyr motifs recognised by anti-phosphotyrosine antibodies used in the immunoprecipitation [40]. Consistent with this idea, a comparative analysis of the identified pTyr sites from the previous immunoprecipitation and the current IMAC/TiO2 enrichment shows the overlap of only 1 phosphorylation site between the two datasets (Figure S2). Comparing our phosphoproteomic datasets with the PhosphoSitePlus database showed that 389 and 394 novel phosphosites were identified in the PazR/A204 and DasR/A204 experiments, respectively (Figure S1B, Table S1 and S2) [30]. The total number of phosphosites identified in our dataset is comparable with previous phosphoproteomic studies (ranging from 2000-5000 phosphosites) where single-shot sample injection into the mass spectrometer was carried out with no additional fractionation [41-45].

Quantitative phosphoproteomic analysis of pazopanib resistance

5420 phosphosites on 1950 proteins were quantified in two or more replicates in the PazR/A204 experiments (Figure 2A). To determine the cellular localisation of phosphorylated proteins which are significantly upregulated in PazR or parental A204 cells, we interrogated our dataset using the Uniprot Keyword database and found that with the exception of the nucleus, phosphorylated proteins across multiple subcellular compartments were increased in PazR cells versus the parental A204 line (Figure 2B). 198 phosphorylation sites on 112 proteins (3.7% of the phosphoproteomic dataset) were significantly upregulated more than 2-times ($>\log_2 +1$) in PazR cells compared to parental A204 cells (Figure 2A).

These phosphoproteins that were upregulated in PazR cells were subjected to ontology enrichment analysis which revealed the enrichment of a number of ontology terms associated with cytoskeletal organisation (Figure 2C). These included “actin-binding”, “LIM domain containing”, and “Calponin homology (CH) domain containing” proteins (Figure 3A) [46-49]. LIM domain-containing proteins comprise AJUBA, CRIP2, LASP1, LMP7, MICALL1, PDLIM7 and TGFB1I1 whilst CH-domain proteins include FLNA, LMO7, MICALL1, NAV2, PLEC and SPECC1 (Figure 3B). This gene ontology enrichment analysis suggests that PazR cells upregulate multiple actin cytoskeletal-regulatory pathways which may play a role in maintaining its drug resistant state.

122 phosphosites on 71 proteins (2.3% of the dataset) were found to be significantly upregulated ($<\log_2 -1$) in the parental A204 cells compared to the PazR cells (Figure 2A) with up to 40% being nuclear proteins (Figure 2B). Ontology analysis of these phosphorylated proteins identified an enrichment of proteins involved in transcription regulation including the ontology terms “transcription regulation”, “transcription”, “transcription activator” and “transcription repressor” (Figure 2C and Figure 3A). These include the transcription factors ETV6, SOX5, SOX6, KLF3, NFIX and DNA binding proteins DNMT1, CDH8, CDH9 and VGLL4 (Figure 3B). Upon interrogation with the STRING database [38], a subset of these proteins showed a well annotated protein-protein interaction network centred around the HDAC1 protein (Figure 3C). The discovery that the phosphorylation of multiple transcription factors is upregulated in SMARCB1-deficient parental A204 rhabdoid tumour cells is consistent with the role of SMARCB1 in organising nucleosome structures surrounding transcriptional start sites in a genome-wide manner [50].

Quantitative phosphoproteomic analysis of dasatinib resistance

5899 phosphosites on 2086 proteins were quantified in two or more biological replicates in the DazR/A204 experiments (Figure 4A). In contrast to the PazR/A204 dataset, both the DasR and parental A204 cell lines show comparable distribution of upregulated

phosphorylated proteins across multiple cellular compartments (Figure 4B). The exception is the nuclear compartment where the parental A204 cells have a slight increase in enrichment over the DasR cells. 279 phosphorylation sites on 157 proteins (4.7% of the dataset) were significantly upregulated more than 2-times in DazR cells compared to parental A204 cells (Figure 4A). Subjecting these upregulated phosphosites to gene ontology enrichment analysis (Figure 4C) finds that the DasR cells shows a distinct spectrum of ontology terms compared to the PazR cells with the enrichment of insulin - and IGF-1R signalling pathway components and PDZ domain containing proteins. The insulin signalling pathway cluster includes the proteins ACACA, ARAF, FASN, IRS1, PRKAR1B, PRKAR2B, RPS6KA1, RPS6KB1 and SHC1 which together form a functional protein-protein interaction network (Figure 5). PDZ domain containing proteins that are upregulated in DasR cells include proteins with a range of cellular functions such as cell migration regulation (AHNAK, AHNAK2, SCRIB), cytoskeletal and tight junction proteins (MYO18A and TJP2), and the sodium/hydrogen exchange cofactor SLC9A3R1 (Figure 5A and B).

294 phosphorylation sites on 157 proteins (5% of the dataset) were found to be upregulated in the parental A204 versus the DasR cells (Figure 4A). Enriched ontology terms include SH3 domain containing proteins (Figure 4C) which play a role in small GTPase regulation and comprise key signalling proteins ARHGEF26, ASAP1, ASAP2, FNBP1L and SRGAP1 (Figure 5A and B). Similar to the PazR/A204 dataset, there was an enrichment of transcriptional regulatory terms which include “transcription repressor” and “interferon regulatory factor” (Figure 4C). These include the transcription factors ETV6, NFATC1, ZNF521 and transcriptional repressors NCOR1, TLE4 and SUDS3 (Figure 5). A subset of these proteins feature as part of a protein-protein interaction network centred around the HDAC3 protein (Figure 5C). The observation that protein-protein interaction networks involving the histone deacetylases (HDACs) are enriched in A204 parental cells in both the PazR/A204 and DasR/A204 experiments (Figure 3C and 5C) is consistent with recent

441 preclinical reports that HDAC inhibitors have therapeutic utility in reducing the proliferation of
442 rhabdoid tumour cells including the A204 line [51-53].
443
444 Comparison of PazR and DasR phosphoproteomic datasets
445 A comparison between the two phosphoproteomic datasets revealed a 70.5% overlap with
446 4683 phosphorylation sites quantified across both resistant cell lines (Figure 6A). Taken
447 together, we find that 21.6% of the phosphoproteome is significantly altered upon the
448 acquisition of secondary resistance in PazR and/or DasR sublines versus the parental A204
449 cells (Figure 6B). Supporting our hypothesis that pazopanib and dasatinib induce different
450 cellular reprogramming effects in the A204 cells, only 2.8% and 1.9% of observed
451 phosphosites are similarly up- and down-regulated, respectively, in both datasets (Figure
452 6B). The 34 upregulated and 36 downregulated phosphosites are detailed in Figure 6C-D.
453
454 Drug response profiling identifies new vulnerabilities in drug resistant cells
455 Inspired by a recent targeted screen to identify drugs capable of overcoming bypass
456 signalling pathways associated with acquired TKI resistance in lung cancer [24], we
457 subjected both resistant lines and the parental A204 cells to short term treatment with a
458 focused panel of 28 small molecule inhibitors at two different doses and measured cell
459 viability. This panel comprised of kinase inhibitors targeting the major cellular signalling
460 pathways important for cancer cell survival as well as inhibitors that target the BET
461 bromodomain proteins (JQ1) and the HSP90 protein (NVP-AUY-922) which are currently in
462 advanced clinical trials.
463
464 Two-way hierarchical clustering of the cell viability data demonstrates that the PazR and
465 DasR cells share a more similar drug response profile compared to parental A204 cells
466 (Figure 7A). As shown in our previous study, the two resistant cell lines are highly sensitive
467 to ponatinib treatment [12]. The screen also showed that the dual mTOR/PI3K inhibitor BEZ-
468 235 sensitized both DasR and PazR which recapitulates the findings of a recent report on

the use of this drug to overcome pazopanib resistance in patient-derived soft tissue sarcoma cells [54]. We also identify several inhibitors that are only effective in the DasR cells including the MEK inhibitor trametinib and to a lesser extent the CDK4/6 inhibitor palbociclib. MEK inhibitors have been shown to overcome drug resistance induced by the paradoxical activation of the MEK/ERK pathway through the weak binding of dasatinib to BRAF and CRAF [55]. The ability of our targeted screen to rediscover several previously identified vulnerabilities associated with pazopanib and dasatinib resistance provides confidence of the broad applicability of this strategy to identify salvage therapies to sensitize TKI-resistant cells.

This screen also uncovered a previously undescribed vulnerability of both PazR and DasR cells to the second generation HSP90 inhibitor NVP-AUY-922 which clustered together with ponatinib [56]. Dose response analysis confirms that PazR and DasR cells are sensitive to treatment with NVP-AUY-922 with IC_{50} values of 45.3 ± 14.3 nM and 28.4 ± 5.9 nM, respectively (Figure 7B and C). Long-term colony formation assays show that low dose NVP-AUY-922 (5nM) is capable of not only sensitizing both PazR and DasR cells but also killing parental A204 cells (Figure 7D and E), suggesting that HSP90 inhibitors may be an effective option both as first-line and salvage therapy in rhabdoid tumours.

Discussion

This study is, to our knowledge, the first phosphoproteomic analysis of acquired resistance to pazopanib and dasatinib. We show that A204 cells that have acquired secondary resistance to pazopanib (PazR) harbour an enrichment of phosphoproteins that play a role in the regulation of actin cytoskeleton dynamics (Figure 3). These include the LIM domain family of proteins CRIP2, LASP1, MICALL1 and PDLIM7 which have previously been shown to be localised in focal adhesion complexes and play important roles in mechanotransduction signalling [46, 57, 58]. In addition, phosphoproteins that contain the CH domain, a 100 amino acid residue domain that binds to actin filaments, are similarly

enriched in PazR cells [48, 49]. Published phosphoproteomic studies have found that melanoma cells with acquired resistance to BRAF inhibitors display elevated levels of phosphoproteins that function in cytoskeletal regulatory pathways [59, 60]. It remains to be determined if the upregulation of cytoskeletal pathways observed in our current study and in the previous melanoma reports is a cause or consequence of the acquisition of drug resistance. However given that this class of proteins is poorly explored as oncology drug targets [61], these phosphoproteomic studies provides a rich source of new candidates for target validation and drug development to overcome drug resistance. In contrast to the PazR cells, acquired resistance to dasatinib in the DasR subline leads to the upregulation of components of the insulin receptor/IGF-1R signalling pathway compared to parental A204 cells (Figure 5). Activation of IGF-1R signalling is a well-established bypass mechanism of resistance to many kinase inhibitors including EGFR, HER2, MEK and BRAF inhibitors [62-66]. Furthermore, intrinsic resistance to dasatinib in a panel of non-small-cell lung cancer cell lines has been causally linked to the upregulation of Insulin-like growth factor (IGF)-binding protein-2 (IGFBP2) which act as carrier proteins for the IGF ligands [67]. Our data suggests that the Insulin receptor/IGF-1R pathway is an actionable target for salvage therapy and further investigation to dissect the contribution of components of this pathway to acquired dasatinib resistance is planned.

One limitation of our study is the relatively modest number of phosphorylation sites identified in our analysis. We quantified ~7000 phosphorylation sites in our experimental dataset (Figure 1B) which is comparable with published reports on single-shot unfractionated samples [42, 44, 45]. In addition, increased precursor ion complexity associated with SILAC labelling results in a decrease in unique phosphopeptide identification [68]. Greater depth of coverage in the phosphoproteome can be achieved with additional pre-fractionation steps [42, 44, 45], and combining orthogonal phosphopeptide enrichment strategies [69, 70]. Another limitation of the study is the focus on phosphoproteomic analysis without accounting for protein abundance changes. In the absence of a deep proteome analysis of the resistant

525 and sensitive cell lines, we are unable to distinguish if the phosphorylation changes
526 observed in our dataset are due to alterations in protein phosphorylation stoichiometry or at
527 the level of total protein expression. Notwithstanding these limitations, our study
528 demonstrates that candidate resistance signalling pathways can be readily identified with
529 this approach.
530
531 Our phosphoproteomic analysis finds that acquired resistance to pazopanib and dasatinib
532 leads to a 6.0% and 9.7% change, respectively, in the quantified phosphoproteome
533 compared to parental A204 cells (Figure 2A and 4A). A recent study by Nagata et al.,
534 showed that acquired resistance to the TKI imatinib in a GIST cell line displayed alterations
535 in ~75% of the phosphoproteome when compared to the parental sensitive cell line [21]. In
536 contrast, a phosphoproteomic analysis by Lee et al., of acquired resistance to the TKI
537 lapatinib in a gastric cancer cell line showed that 5% of the phosphoproteome was
538 significantly altered versus the parental cells from which resistance was derived [20]. The
539 low percentage of phosphorylation changes observed in our study may be due to a number
540 of factors. One reason could be that the depth of phosphoproteome coverage is less
541 comprehensive in our analysis and that we are only sampling the most abundant
542 phosphoproteins in the cell, although this is unlikely given that the study by Nagata et al.,
543 identified ~1000 phosphoserine/threonine sites with a 75% difference observed while Lee et
544 al., quantified 6500 phosphosites with only 5% alterations seen. Another contributing factor
545 is that the underlying genomic drivers of the cell lines used in the different studies are
546 distinct. Unlike the GIST and gastric cell lines used in the previous studies, the A204
547 rhabdoid tumour cell line has a very simple genome where the loss of the SWI/SNF
548 chromatin remodelling subunit SMARCB1 is the only known cancer-associated driver [12,
549 71-74]. It is plausible that loss of SMARCB1 may be sufficient to drive acquired TKI
550 resistance with limited alterations in the phosphoproteome. Finally it is also possible that
551 different TKIs reprogram cellular signalling networks to achieve drug resistance using distinct
552 mechanisms [4, 75, 76].

The targeted drug profiling analysis identified the HSP90 inhibitor NVP-AUY-922 as a novel means to overcome pazopanib and dasatinib resistance (Figure 7). The small molecule inhibitor panel that we employed was designed to block a range of distinct bypass pathways that have previously been associated with TKI resistance [24]. We show that AUY-922 is capable of not only overcoming acquired resistance in the form of salvage therapy, but also has utility when applied in the first-line setting (Figure 7C). HSP90 inhibitors have been deployed as salvage therapy in clinical trials for TKI-resistant lung cancer and GIST with varying results [77, 78]. The rationale for this approach is based on pre-clinical evidence that cancer cells are dependent on HSP90 for stabilising client proteins such as TKI resistance-associated mutants and kinases responsible for driving bypass signalling in cancer cells [79, 80]. Consequently inhibition of HSP90 has the potential to simultaneously block multiple resistance mechanisms in the context of salvage therapy [80]. The mechanism for the activity of AUY922 in sensitizing the PazR and DasR cells and the specific client proteins involved in mediating drug sensitivity remain unclear and will be the focus of future studies.

In summary, we have performed a phosphoproteomic analysis to determine the signalling pathways associated with acquired resistance to pazopanib and dasatinib. We also demonstrate that PazR and DasR cells are sensitive to the HSP90 inhibitor NVP-AUY-922. This study provides a useful resource for future studies investigating the determinants of pazopanib and dasatinib resistance; and identifies a new therapeutic strategy of inhibiting HSP90 function for further evaluation as a means of overcoming pazopanib and dasatinib resistance and tumour recurrence in multiple cancer types.

Acknowledgements

This work was supported by grants to PHH from the Institute of Cancer Research, Cancer Research UK (C36478/A19281), Sarcoma UK (003.2014), Royal Marsden Cancer Charity. SV is supported by an ICR studentship.

References

[1] Lemmon MA, Schlessinger J. Cell signaling by receptor tyrosine kinases. Cell. 2010;141:1117-34.

[2] Levitzki A. Tyrosine kinase inhibitors: views of selectivity, sensitivity, and clinical performance. Annu Rev Pharmacol Toxicol. 2013;53:161-85.

[3] Sierra JR, Cepero V, Giordano S. Molecular mechanisms of acquired resistance to tyrosine kinase targeted therapy. Mol Cancer. 2010;9:75.

[4] Gainor JF, Shaw AT. Emerging paradigms in the development of resistance to tyrosine kinase inhibitors in lung cancer. J Clin Oncol. 2013;31:3987-96.

[5] Xu AM, Huang PH. Receptor tyrosine kinase coactivation networks in cancer. Cancer Res. 2010;70:3857-60.

[6] Vyse S, Howitt A, Huang PH. Exploiting Synthetic Lethality and Network Biology to Overcome EGFR Inhibitor Resistance in Lung Cancer. J Mol Biol. 2017.

[7] Hata AN, Niederst MJ, Archibald HL, Gomez-Caraballo M, Siddiqui FM, Mulvey HE, et al. Tumor cells can follow distinct evolutionary paths to become resistant to epidermal growth factor receptor inhibition. Nat Med. 2016;22:262-9.

[8] Ramirez M, Rajaram S, Steininger RJ, Osipchuk D, Roth MA, Morinishi LS, et al. Diverse drug-resistance mechanisms can emerge from drug-tolerant cancer persister cells. Nat Commun. 2016;7:10690.

[9] Kitagawa D, Yokota K, Gouda M, Narumi Y, Ohmoto H, Nishiwaki E, et al. Activity-based kinase profiling of approved tyrosine kinase inhibitors. Genes Cells. 2013;18:110-22.

[10] Anastassiadis T, Deacon SW, Devarajan K, Ma H, Peterson JR. Comprehensive assay of kinase catalytic activity reveals features of kinase inhibitor selectivity. Nat Biotechnol. 2011;29:1039-45.

[11] Davis MI, Hunt JP, Herrgard S, Ciceri P, Wodicka LM, Pallares G, et al. Comprehensive analysis of kinase inhibitor selectivity. Nat Biotechnol. 2011;29:1046-51.

[12] Wong JP, Todd JR, Finetti MA, McCarthy F, Broncel M, Vyse S, et al. Dual Targeting of PDGFRalpha and FGFR1 Displays Synergistic Efficacy in Malignant Rhabdoid Tumors. Cell Rep. 2016;17:1265-75.

[13] Motzer RJ, Hutson TE, Cella D, Reeves J, Hawkins R, Guo J, et al. Pazopanib versus sunitinib in metastatic renal-cell carcinoma. N Engl J Med. 2013;369:722-31.

[14] van der Graaf WT, Blay JY, Chawla SP, Kim DW, Bui-Nguyen B, Casali PG, et al. Pazopanib for metastatic soft-tissue sarcoma (PALETTE): a randomised, double-blind, placebo-controlled phase 3 trial. Lancet. 2012;379:1879-86.

[15] Talpaz M, Shah NP, Kantarjian H, Donato N, Nicoll J, Paquette R, et al. Dasatinib in imatinib-resistant Philadelphia chromosome-positive leukemias. N Engl J Med. 2006;354:2531-41.

620 [16] Kantarjian H, Shah NP, Hochhaus A, Cortes J, Shah S, Ayala M, et al. Dasatinib versus
621 imatinib in newly diagnosed chronic-phase chronic myeloid leukemia. N Engl J Med.
622 2010;362:2260-70.

623 [17] Yang W, Soares J, Greninger P, Edelman EJ, Lightfoot H, Forbes S, et al. Genomics of
624 Drug Sensitivity in Cancer (GDSC): a resource for therapeutic biomarker discovery in cancer
625 cells. Nucleic Acids Res. 2013;41:D955-61.

626 [18] Dazert E, Colombi M, Boldanova T, Moes S, Adametz D, Quagliata L, et al. Quantitative
627 proteomics and phosphoproteomics on serial tumor biopsies from a sorafenib-treated HCC
628 patient. Proc Natl Acad Sci U S A. 2016;113:1381-6.

629 [19] Yoshida T, Zhang G, Smith MA, Lopez AS, Bai Y, Li J, et al. Tyrosine
630 phosphoproteomics identifies both codrivers and cotargeting strategies for T790M-related
631 EGFR-TKI resistance in non-small cell lung cancer. Clin Cancer Res. 2014;20:4059-74.

632 [20] Lee YY, Kim HP, Kang MJ, Cho BK, Han SW, Kim TY, et al. Phosphoproteomic analysis
633 identifies activated MET-axis PI3K/AKT and MAPK/ERK in lapatinib-resistant cancer cell
634 line. Exp Mol Med. 2013;45:e64.

635 [21] Nagata K, Kawakami T, Kurata Y, Kimura Y, Suzuki Y, Nagata T, et al. Augmentation of
636 multiple protein kinase activities associated with secondary imatinib resistance in
637 gastrointestinal stromal tumors as revealed by quantitative phosphoproteome analysis. J
638 Proteomics. 2015;115:132-42.

639 [22] Winter GE, Rix U, Carlson SM, Gleixner KV, Grebien F, Gridling M, et al. Systems-
640 pharmacology dissection of a drug synergy in imatinib-resistant CML. Nat Chem Biol.
641 2012;8:905-12.

642 [23] Noujaim J, Payne LS, Judson I, Jones RL, Huang PH. Phosphoproteomics in
643 translational research: a sarcoma perspective. Ann Oncol. 2016;27:787-94.

644 [24] Crystal AS, Shaw AT, Sequist LV, Friboulet L, Niederst MJ, Lockerman EL, et al.
645 Patient-derived models of acquired resistance can identify effective drug combinations for
646 cancer. Science. 2014;346:1480-6.

647 [25] Iwai LK, Payne LS, Luczynski MT, Chang F, Xu H, Clinton RW, et al.
648 Phosphoproteomics of collagen receptor networks reveals SHP-2 phosphorylation
649 downstream of wild-type DDR2 and its lung cancer mutants. Biochem J. 2013;454:501-13.

650 [26] Cox J, Mann M. MaxQuant enables high peptide identification rates, individualized
651 p.p.b.-range mass accuracies and proteome-wide protein quantification. Nat Biotechnol.
652 2008;26:1367-72.

653 [27] Cox J, Neuhauser N, Michalski A, Scheltema RA, Olsen JV, Mann M. Andromeda: a
654 peptide search engine integrated into the MaxQuant environment. J Proteome Res.
655 2011;10:1794-805.

656 [28] Tyanova S, Temu T, Sinitcyn P, Carlson A, Hein MY, Geiger T, et al. The Perseus
657 computational platform for comprehensive analysis of (prote)omics data. Nat Methods.
658 2016;13:731-40.

659 [29] Vizcaino JA, Csordas A, Del-Toro N, Dianes JA, Griss J, Lavidas I, et al. 2016 update of
660 the PRIDE database and its related tools. Nucleic Acids Res. 2016.

[30] Hornbeck PV, Zhang B, Murray B, Kornhauser JM, Latham V, Skrzypek E. PhosphoSitePlus, 2014: mutations, PTMs and recalibrations. Nucleic Acids Res. 2015;43:D512-20.

[31] Huang da W, Sherman BT, Lempicki RA. Systematic and integrative analysis of large gene lists using DAVID bioinformatics resources. Nat Protoc. 2009;4:44-57.

[32] Kanehisa M, Furumichi M, Tanabe M, Sato Y, Morishima K. KEGG: new perspectives on genomes, pathways, diseases and drugs. Nucleic Acids Res. 2017;45:D353-D61.

[33] UniProt: the universal protein knowledgebase. Nucleic Acids Res. 2017;45:D158-D69.

[34] Finn RD, Attwood TK, Babbitt PC, Bateman A, Bork P, Bridge AJ, et al. InterPro in 2017-beyond protein family and domain annotations. Nucleic Acids Res. 2017;45:D190-D9.

[35] Letunic I, Doerks T, Bork P. SMART: recent updates, new developments and status in 2015. Nucleic Acids Res. 2015;43:D257-60.

[36] Tatusov RL, Fedorova ND, Jackson JD, Jacobs AR, Kiryutin B, Koonin EV, et al. The COG database: an updated version includes eukaryotes. BMC Bioinformatics. 2003;4:41.

[37] Shannon P, Markiel A, Ozier O, Baliga NS, Wang JT, Ramage D, et al. Cytoscape: a software environment for integrated models of biomolecular interaction networks. Genome Res. 2003;13:2498-504.

[38] Szklarczyk D, Morris JH, Cook H, Kuhn M, Wyder S, Simonovic M, et al. The STRING database in 2017: quality-controlled protein-protein association networks, made broadly accessible. Nucleic Acids Res. 2017;45:D362-D8.

[39] Ubersax JA, Ferrell JE, Jr. Mechanisms of specificity in protein phosphorylation. Nat Rev Mol Cell Biol. 2007;8:530-41.

[40] Tinti M, Nardozza AP, Ferrari E, Sacco F, Corallino S, Castagnoli L, et al. The 4G10, pY20 and p-TYR-100 antibody specificity: profiling by peptide microarrays. N Biotechnol. 2012;29:571-7.

[41] Zahari MS, Wu X, Pinto SM, Nirujogi RS, Kim MS, Fetics B, et al. Phosphoproteomic profiling of tumor tissues identifies HSP27 Ser82 phosphorylation as a robust marker of early ischemia. Sci Rep. 2015;5:13660.

[42] Lawrence RT, Searle BC, Llovet A, Villen J. Plug-and-play analysis of the human phosphoproteome by targeted high-resolution mass spectrometry. Nat Methods. 2016;13:431-4.

[43] Bensimon A, Schmidt A, Ziv Y, Elkon R, Wang SY, Chen DJ, et al. ATM-dependent and -independent dynamics of the nuclear phosphoproteome after DNA damage. Sci Signal. 2010;3:rs3.

[44] Matheron L, van den Toorn H, Heck AJ, Mohammed S. Characterization of biases in phosphopeptide enrichment by Ti(4+)-immobilized metal affinity chromatography and TiO2 using a massive synthetic library and human cell digests. Anal Chem. 2014;86:8312-20.

[45] Ruprecht B, Koch H, Medard G, Mundt M, Kuster B, Lemeer S. Comprehensive and reproducible phosphopeptide enrichment using iron immobilized metal ion affinity chromatography (Fe-IMAC) columns. Mol Cell Proteomics. 2015;14:205-15.

[46] Smith MA, Hoffman LM, Beckerle MC. LIM proteins in actin cytoskeleton mechanoresponse. Trends Cell Biol. 2014;24:575-83.

[47] Jarvinen PM, Laiho M. LIM-domain proteins in transforming growth factor beta-induced epithelial-to-mesenchymal transition and myofibroblast differentiation. Cell Signal. 2012;24:819-25.

[48] Sjoblom B, Ylanne J, Djinovic-Carugo K. Novel structural insights into F-actin-binding and novel functions of calponin homology domains. Curr Opin Struct Biol. 2008;18:702-8.

[49] Korenbaum E, Rivero F. Calponin homology domains at a glance. J Cell Sci. 2002;115:3543-5.

[50] Tolstorukov MY, Sansam CG, Lu P, Koellhoffer EC, Helming KC, Alver BH, et al. Swi/Snf chromatin remodeling/tumor suppressor complex establishes nucleosome occupancy at target promoters. Proc Natl Acad Sci U S A. 2013;110:10165-70.

[51] Muscat A, Popovski D, Jayasekara WS, Rossello FJ, Ferguson M, Marini KD, et al. Low-Dose Histone Deacetylase Inhibitor Treatment Leads to Tumor Growth Arrest and Multi-Lineage Differentiation of Malignant Rhabdoid Tumors. Clin Cancer Res. 2016;22:3560-70.

[52] Kerl K, Ries D, Unland R, Borchert C, Moreno N, Hasselblatt M, et al. The histone deacetylase inhibitor SAHA acts in synergism with fenretinide and doxorubicin to control growth of rhabdoid tumor cells. BMC Cancer. 2013;13:286.

[53] Knipstein JA, Birks DK, Donson AM, Alimova I, Foreman NK, Vibhakar R. Histone deacetylase inhibition decreases proliferation and potentiates the effect of ionizing radiation in atypical teratoid/rhabdoid tumor cells. Neuro Oncol. 2012;14:175-83.

[54] Kim HK, Kim SY, Lee SJ, Kang M, Kim ST, Jang J, et al. BEZ235 (PIK3/mTOR inhibitor) Overcomes Pazopanib Resistance in Patient-Derived Refractory Soft Tissue Sarcoma Cells. Transl Oncol. 2016;9:197-202.

[55] Packer LM, Rana S, Hayward R, O'Hare T, Eide CA, Rebocho A, et al. Nilotinib and MEK inhibitors induce synthetic lethality through paradoxical activation of RAF in drug-resistant chronic myeloid leukemia. Cancer Cell. 2011;20:715-27.

[56] Eccles SA, Massey A, Raynaud FI, Sharp SY, Box G, Valenti M, et al. NVP-AUY922: a novel heat shock protein 90 inhibitor active against xenograft tumor growth, angiogenesis, and metastasis. Cancer Res. 2008;68:2850-60.

[57] Schiller HB, Friedel CC, Boulegue C, Fassler R. Quantitative proteomics of the integrin adhesome show a myosin II-dependent recruitment of LIM domain proteins. EMBO Rep. 2011;12:259-66.

[58] Kuo JC, Han X, Hsiao CT, Yates JR, 3rd, Waterman CM. Analysis of the myosin-II-responsive focal adhesion proteome reveals a role for beta-Pix in negative regulation of focal adhesion maturation. Nat Cell Biol. 2011;13:383-93.

[59] Parker R, Vella LJ, Xavier D, Amirkhani A, Parker J, Cebon J, et al. Phosphoproteomic Analysis of Cell-Based Resistance to BRAF Inhibitor Therapy in Melanoma. Front Oncol. 2015;5:95.

[60] Girotti MR, Pedersen M, Sanchez-Laorden B, Viros A, Turajlic S, Niculescu-Duvaz D, et al. Inhibiting EGF receptor or SRC family kinase signaling overcomes BRAF inhibitor resistance in melanoma. Cancer Discov. 2013;3:158-67.

[61] Patel MN, Halling-Brown MD, Tym JE, Workman P, Al-Lazikani B. Objective assessment of cancer genes for drug discovery. Nat Rev Drug Discov. 2013;12:35-50.

[62] Cortot AB, Repellin CE, Shimamura T, Capelletti M, Zejnullahu K, Ercan D, et al. Resistance to irreversible EGF receptor tyrosine kinase inhibitors through a multistep mechanism involving the IGF1R pathway. Cancer Res. 2013;73:834-43.

[63] Guix M, Faber AC, Wang SE, Olivares MG, Song Y, Qu S, et al. Acquired resistance to EGFR tyrosine kinase inhibitors in cancer cells is mediated by loss of IGF-binding proteins. J Clin Invest. 2008;118:2609-19.

[64] Nahta R, Yuan LX, Zhang B, Kobayashi R, Esteva FJ. Insulin-like growth factor-I receptor/human epidermal growth factor receptor 2 heterodimerization contributes to trastuzumab resistance of breast cancer cells. Cancer Res. 2005;65:11118-28.

[65] Villanueva J, Vultur A, Lee JT, Somasundaram R, Fukunaga-Kalabis M, Cipolla AK, et al. Acquired resistance to BRAF inhibitors mediated by a RAF kinase switch in melanoma can be overcome by cotargeting MEK and IGF-1R/PI3K. Cancer Cell. 2010;18:683-95.

[66] Denduluri SK, Idowu O, Wang Z, Liao Z, Yan Z, Mohammed MK, et al. Insulin-like growth factor (IGF) signaling in tumorigenesis and the development of cancer drug resistance. Genes Dis. 2015;2:13-25.

[67] Lu H, Wang L, Gao W, Meng J, Dai B, Wu S, et al. IGFBP2/FAK pathway is causally associated with dasatinib resistance in non-small cell lung cancer cells. Mol Cancer Ther. 2013;12:2864-73.

[68] Ong SE. The expanding field of SILAC. Anal Bioanal Chem. 2012;404:967-76.

[69] Engholm-Keller K, Hansen TA, Palmisano G, Larsen MR. Multidimensional strategy for sensitive phosphoproteomics incorporating protein prefractionation combined with SIMAC, HILIC, and TiO(2) chromatography applied to proximal EGF signaling. J Proteome Res. 2011;10:5383-97.

[70] Vyse S, Desmond H, Huang PH. Advances in mass spectrometry based strategies to study receptor tyrosine kinases. IUCrJ. 2017;4:119-30.

[71] Chou TC, Talalay P. Quantitative analysis of dose-effect relationships: the combined effects of multiple drugs or enzyme inhibitors. Adv Enzyme Regul. 1984;22:27-55.

[72] Johann PD, Erkek S, Zapatka M, Kerl K, Buchhalter I, Hovestadt V, et al. Atypical Teratoid/Rhabdoid Tumors Are Comprised of Three Epigenetic Subgroups with Distinct Enhancer Landscapes. Cancer Cell. 2016;29:379-93.

[73] Lee RS, Stewart C, Carter SL, Ambrogio L, Cibulskis K, Sougnez C, et al. A remarkably simple genome underlies highly malignant pediatric rhabdoid cancers. J Clin Invest. 2012;122:2983-8.

[74] Huang PH. Targeting SWI/SNF mutant cancers with tyrosine kinase inhibitor therapy. Expert Rev Anticancer Ther. 2017;17:1-3.

[75] Tan AC, Vyse S, Huang PH. Exploiting receptor tyrosine kinase co-activation for cancer therapy. Drug Discov Today. 2017;22:72-84.

[76] Bonanno L, Jirillo A, Favaretto A. Mechanisms of acquired resistance to epidermal growth factor receptor tyrosine kinase inhibitors and new therapeutic perspectives in non small cell lung cancer. Curr Drug Targets. 2011;12:922-33.

[77] Sequist LV, Gettinger S, Senzer NN, Martins RG, Janne PA, Lilenbaum R, et al. Activity of IPI-504, a novel heat-shock protein 90 inhibitor, in patients with molecularly defined non-small-cell lung cancer. J Clin Oncol. 2010;28:4953-60.

[78] Demitri GD, Heinrich MC, Chmielowski B, Morgan JA, George S, Bradley R, et al. An open-label phase II study of the Hsp90 inhibitor ganetespid (STA-9090) in patients (pts) with metastatic and/or unresectable GIST. J Clin Oncol. 2011;29:10011.

[79] Workman P, Burrows F, Neckers L, Rosen N. Drugging the cancer chaperone HSP90: combinatorial therapeutic exploitation of oncogene addiction and tumor stress. Ann N Y Acad Sci. 2007;1113:202-16.

[80] Proia DA, Bates RC. Ganetespib and HSP90: translating preclinical hypotheses into clinical promise. Cancer Res. 2014;74:1294-300.

Figure Legends

Figure 1. Experimental outline and phosphoprotome dataset overview. (A) Dose response curve of A204 parental and PazR cells to pazopanib and A204 parental and DasR cells to dasatinib respectively. (B) Schematic of sample preparation workflow. Pazopanib and dasatinib resistant A204 cell lines (PazR & DasR respectively) were generated and heavy SILAC labelled as previously described [12]. A204 parental cells were light SILAC labelled. After cell lysis, either heavy PazR or DasR were mixed 1:1 with light A204 parental lysate then reduced, alkylated and trypsin digested. The resulting peptides underwent phospho-tyrosine (pTyr) peptide immunoprecipitation, data previously published [12]. The supernatant from the immunoprecipitation was further enriched with immobilised metal affinity chromatography (IMAC) or titanium dioxide (TiO_2) prior to liquid chromatography tandem mass spectrometry analysis (LC MS/MS). (C) Venn diagrams show distribution of phosphorylation sites across three biological replicates (R1, R2 and R3) in PazR/A204 and DasR/A204 experiments..

Figure 2. Phosphoproteomic profile of PazR versus A204 parental cells. (A) Volcano plot depicting the phosphoproteome of PazR versus A204 parental cells. All ratios were median-normalised and $\log_2$ transformed. A one sample t-test was performed where the null hypothesis was equal to 0. The statistical significance was $-\log_{10}$ transformed (y-axis) and plotted against the t-test difference (x-axis). Phosphosites that display at least 2-times increase in PazR (red) or increase in A204 parental (blue) with $p < 0.05$ are indicated. Legend shows percentage of phosphosites that were up-regulated in PazR cells or A204 parental cells as well as phosphosites that displayed no change between the two cell lines. (B) Uniprot keyword annotation terms linked to either statistically significant PazR or A204 parental up-regulated phosphoproteins generated using the DAVID functional annotation tool [31]. (C) Annotation enrichment analysis of phosphoproteins up-regulated in either the PazR or A204 parental cells compared against the human genome using DAVID. The resultant p values of each term were $-\log_{10}$ transformed. Multiple hypothesis testing was controlled using a Benjamini-Hochburg FDR threshold of 0.1.

Figure 3. Biological function analysis of PazR versus A204 parental cells. (A) Annotation enrichment analysis of PazR and A204 parental up-regulated phosphoproteins using the DAVID functional annotation tool. Network maps represent clusters of annotation terms from different databases with associated function. Nodes represent each term and the connecting line their association; line thickness is number of overlapping proteins. The inner and outer nodes are PazR and A204 parental datasets respectively. Node size represents the number of proteins annotated with that term. The colour intensity of the node represents the significance of enrichment and grey depicts no proteins. (B) Heat map of proteins in network cluster based on the Log_2(PazR/A204) SILAC ratio. (C) An association network of proteins from the 'transcription' cluster analysed through the STRING application. Blue coloured proteins are from the cluster list and grey are added STRING interactors. Line thickness portrays the STRING calculated association confidence.

Figure 4. Phosphoproteomic profile of DasR versus A204 parental cells. (A) Volcano plot depicting the phosphoproteome of DasR versus A204 parental cells. All ratios were median-normalised and $\log_2$ transformed. A one sample t-test was performed where the null hypothesis was equal to 0. The statistical significance was $-\log_{10}$ transformed (y-axis) and plotted against the t-test difference (x-axis). Phosphosites that display at least 2-times increase in DasR (red) or increase in A204 parental (blue) with $p < 0.05$ are indicated. Legend shows percentage of phosphosites that were up-regulated in DasR cells or A204 parental cells as well as phosphosites that displayed no change between the two cell lines. (B) Uniprot keyword annotation terms linked to either statistically significant DasR or A204 parental up-regulated phosphoproteins generated using the DAVID functional annotation tool [31]. (C) Annotation enrichment analysis of phosphoproteins up-regulated in either the DasR or A204 parental cells compared against the human genome using the DAVID application. The resultant p values of each term were $-\log_{10}$ transformed. Multiple hypothesis testing was controlled using a Benjamini-Hochburg FDR threshold of 0.1.

Figure 5. Biological function analysis of DasR versus A204 parental cells. (A) Annotation enrichment analysis of DasR and A204 parental up-regulated phosphoproteins using the DAVID functional annotation tool. Network maps represent clusters of annotation terms from different databases with associated function. Nodes represent each term and the connecting line their association; line thickness is number of overlapping proteins. The inner and outer node are DasR and A204 parental datasets respectively. Node size represents the number of proteins annotated with that term. The colour intensity of the node represents the significance of enrichment and grey depicts no proteins. (B) Heat map of proteins in network cluster based on the Log_2(DasR/A204) SILAC ratio. (C) An association network of proteins from the 'insulin signalling' and 'transcription' clusters were analysed through the STRING application. Red or blue coloured proteins are from the cluster lists and grey are added STRING interactors. Line thickness portrays the STRING calculated association confidence.

Figure 6. Comparative assessment of PazR and DasR cells. (A) Venn diagram to show overlap of phosphosites between the PazR and DasR datasets in at least 2 out of 3 biological replicates. (B) A pie chart distribution using only overlapping phosphosites of both PazR and DasR. Categories include: 'Up' (at least 2-times up-regulated versus parental), 'down' (at least 2-times down-regulated versus parental) and 'no change' (less than 2-times up-regulated and more than 2-times down-regulated). A statistical significance cut-off (p-value < 0.05) was then applied and the overlap between (C) up- or (D) down-regulated (at least 2-times) in PazR and DasR lines compared to A204 parental cells phosphorylation sites are shown.

Figure 7. Drug profiling analysis of in A204 parental and resistant cell lines.

(A) Heatmap depicting two-way hierarchical clustering of cell viability data in drug screen. A204 parental, pazopanib resistant and dasatinib cell lines were seeded in 96 well plates and viability was measured using Cell Titer Glo following 72h of treatment with 28 small molecule inhibitors at 100nM and 500nM (or 10nM and 50nM for NVP-AUY-922). Two-way hierarchical clustering using Euclidean distance was performed. (B) Dose response curve of PazR cells to pazopanib or NVP-AUY-922 treatment. (C) Dose response curve of DasR cells to dasatinib or NVP-AUY-922 treatment. For (A), (B) and (C) cell viability is normalised to DMSO control and values represent mean ± SD (n=2 or 3). Colony formation assays comparing (A) A204 parental and pazopanib resistant and (B) A204 parental and dasatinib resistant cell lines in the presence of drug. Cell lines were seeded at low density (10,000 cells / well) in a 6 well plate. After 2 weeks of treatment with inhibitors at the indicated doses, cells were fixed and colonies were stained using crystal violet for visualisation.

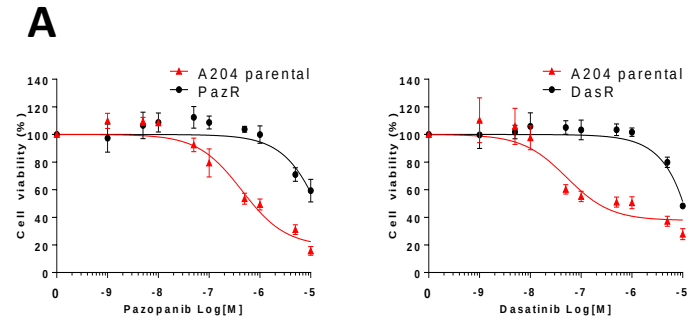
A
A204 parental
PazR
Cell viability (%)
Pazopanib Log[M]
A204 parental
DasR
Cell viability (%)
Dasatinib Log[M]

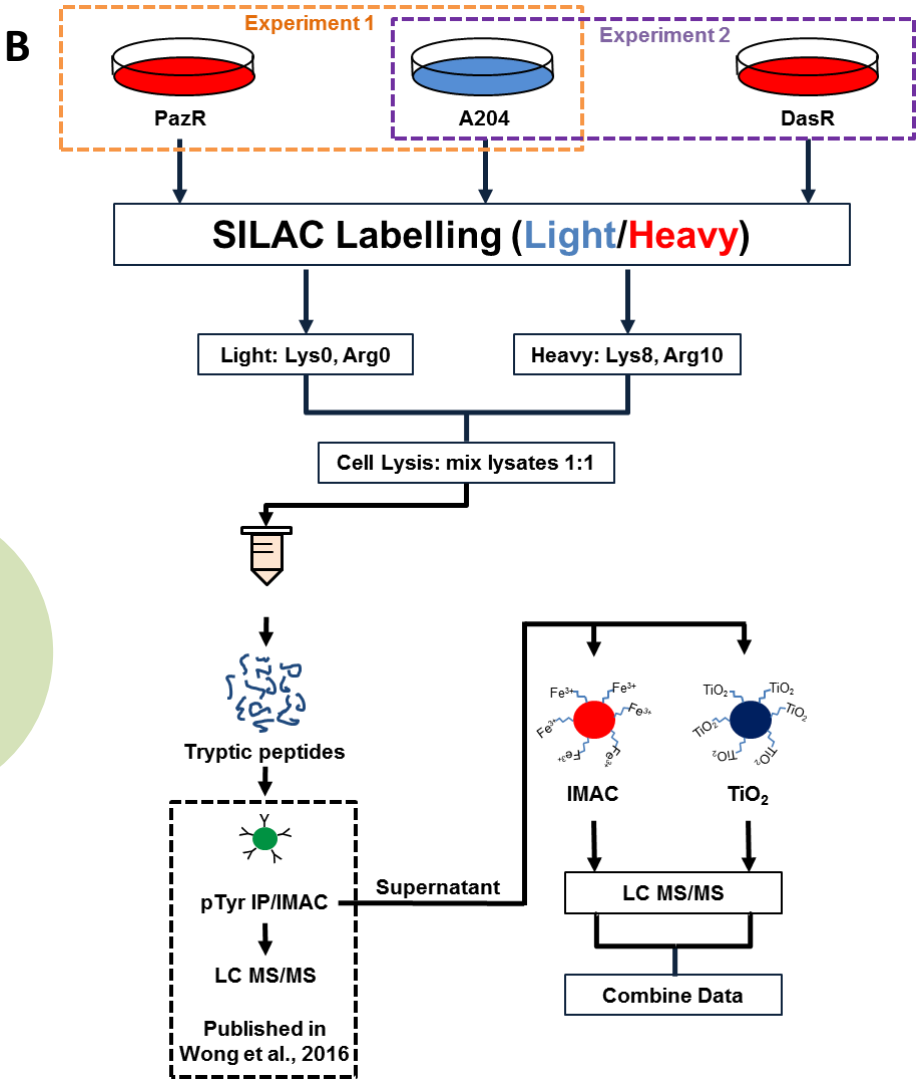
B
Experiment 1
Experiment 2
PazR
A204
DasR
SILAC Labelling (Light/Heavy)
Light: Lys0, Arg0
Heavy: Lys8, Arg10
Cell Lysis: mix lysates 1:1
Tryptic peptides
pTyr IP/IMAC
LC MS/MS
Published in Wong et al., 2016
Supernatant
IMAC
TiO2
LC MS/MS
Combine Data

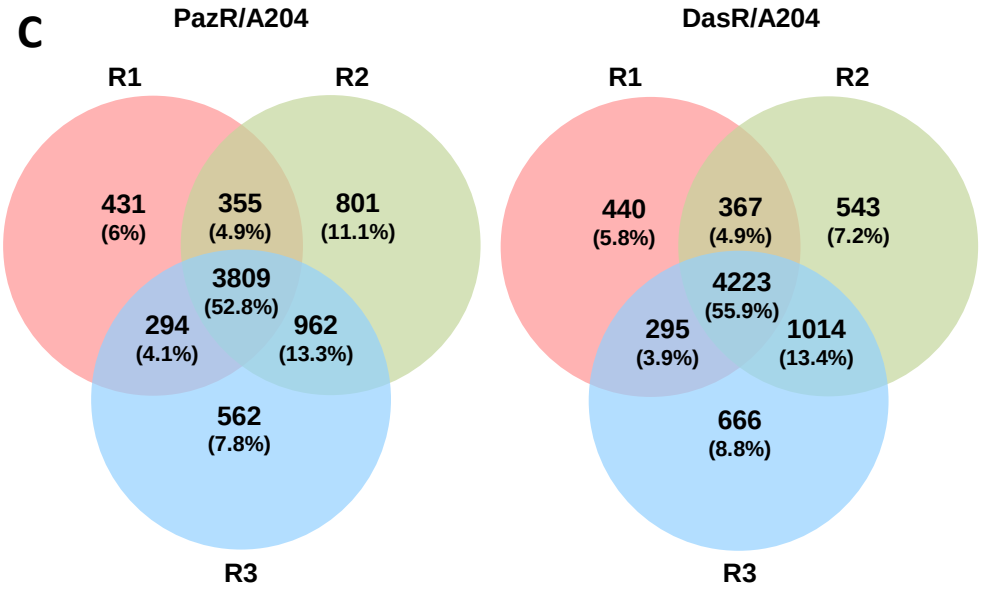
C
PazR/A204
R1
R2
R3
431 (6%)
355 (4.9%)
801 (11.1%)
3809 (52.8%)
294 (4.1%)
962 (13.3%)
562 (7.8%)
DasR/A204
R1
R2
R3
440 (5.8%)
367 (4.9%)
543 (7.2%)
4223 (55.9%)
295 (3.9%)
1014 (13.4%)
666 (8.8%)

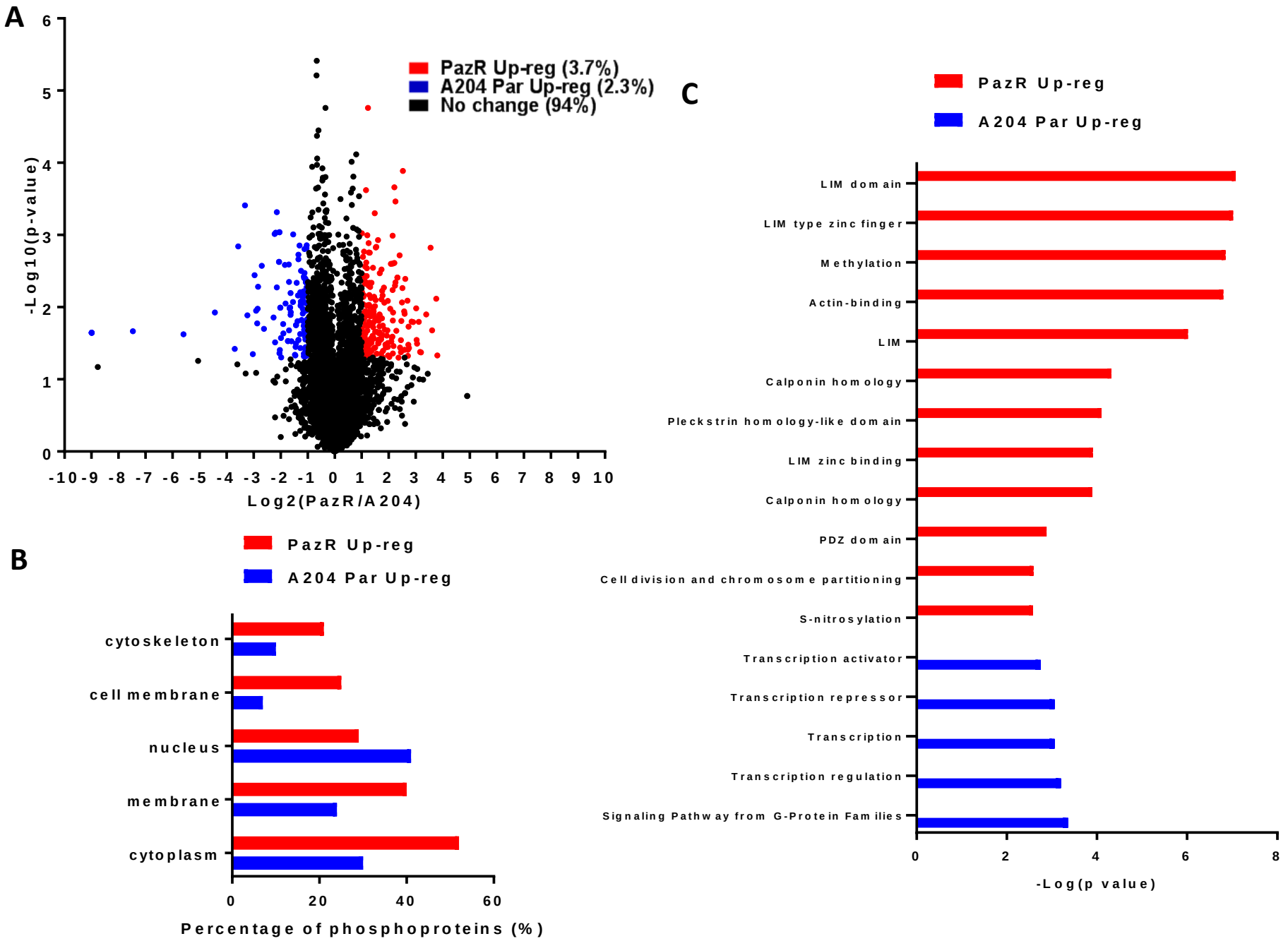
A
PazR Up-reg (3.7%)
A204 Par Up-reg (2.3%)
No change (94%)
-Log10(p-value)
Log2(PazR/A204)
B
PazR Up-reg
A204 Par Up-reg
cytoskeleton
cell membrane
nucleus
membrane
cytoplasm
Percentage of phosphoproteins (%)
C
PazR Up-reg
A204 Par Up-reg
LIM domain
LIM type zinc finger
Methylation
Actin-binding
LIM
Calponin homology
Pleckstrin homology-like domain
LIM zinc binding
Calponin homology
PDZ domain
Cell division and chromosome partitioning
S-nitrosylation
Transcription activator
Transcription repressor
Transcription
Transcription regulation
Signaling Pathway from G-Protein Families
-Log(p value)

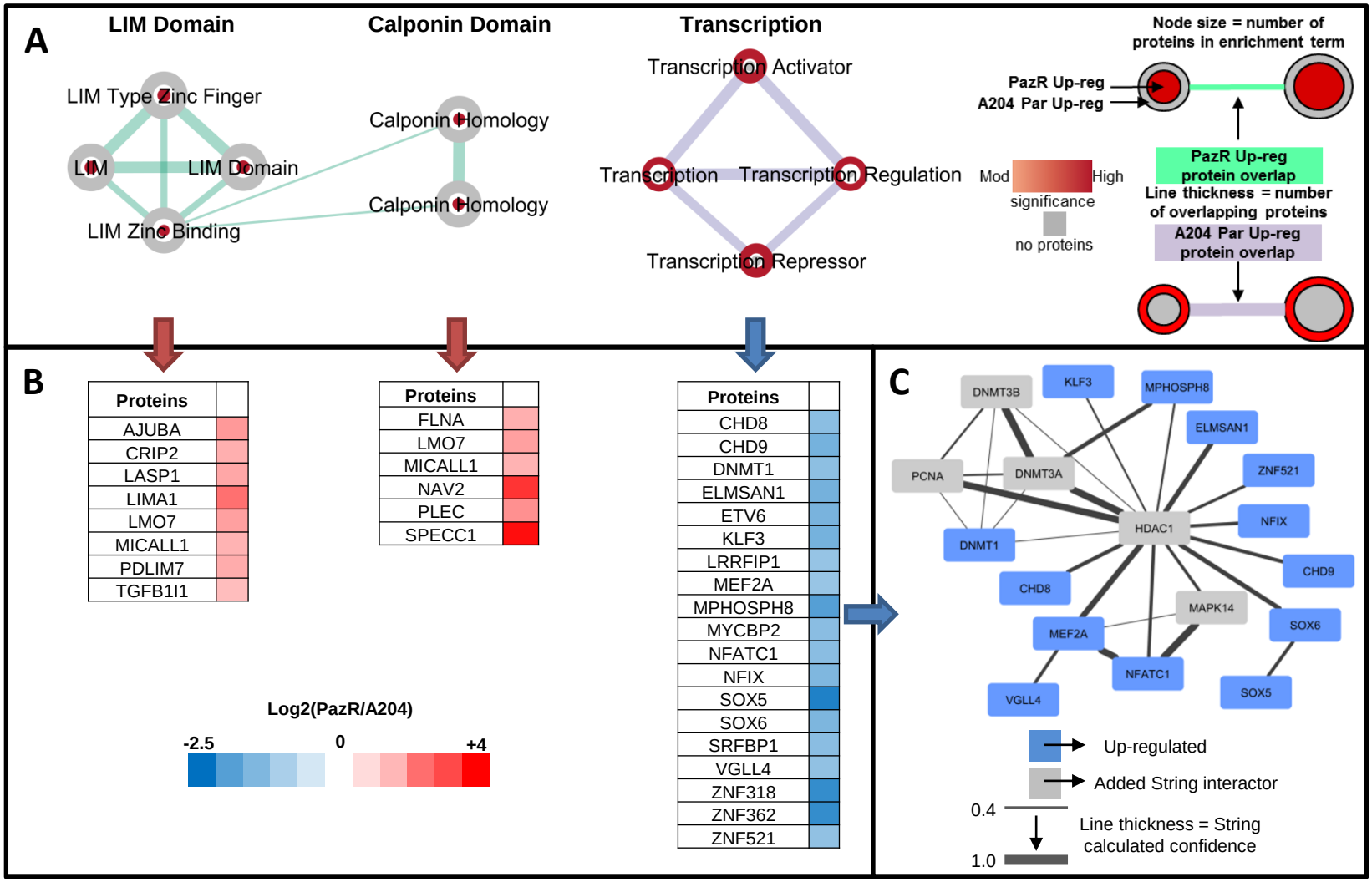
A
LIM Domain
Calponin Domain
Transcription
LIM Type Zinc Finger
LIM
LIM Domain
LIM Zinc Binding
Calponin Homology
Calponin Homology
Transcription Activator
Transcription
Transcription Regulation
Transcription Repressor
Node size = number of proteins in enrichment term
PazR Up-reg
A204 Par Up-reg
PazR Up-reg protein overlap
Line thickness = number of overlapping proteins
A204 Par Up-reg protein overlap
Mod
High
significance
no proteins
B
Proteins
AJUBA
CRIP2
LASP1
LIMA1
LMO7
MICALL1
PDLIM7
TGFB1I1
Proteins
FLNA
LMO7
MICALL1
NAV2
PLEC
SPECC1
Proteins
CHD8
CHD9
DNMT1
ELMSAN1
ETV6
KLF3
LRRFIP1
MEF2A
MPHOSPH8
MYCBP2
NFATC1
NFIX
SOX5
SOX6
SRFBP1
VGLL4
ZNF318
ZNF362
ZNF521
Log2(PazR/A204)
-2.5
0
+4
C
DNMT3B
KLF3
MPHOSPH8
ELMSAN1
PCNA
DNMT3A
ZNF521
HDAC1
NFIX
DNMT1
CHD9
CHD8
MAPK14
SOX6
MEF2A
NFATC1
SOX5
VGLL4
Up-regulated
Added String interactor
0.4
1.0
Line thickness = String calculated confidence

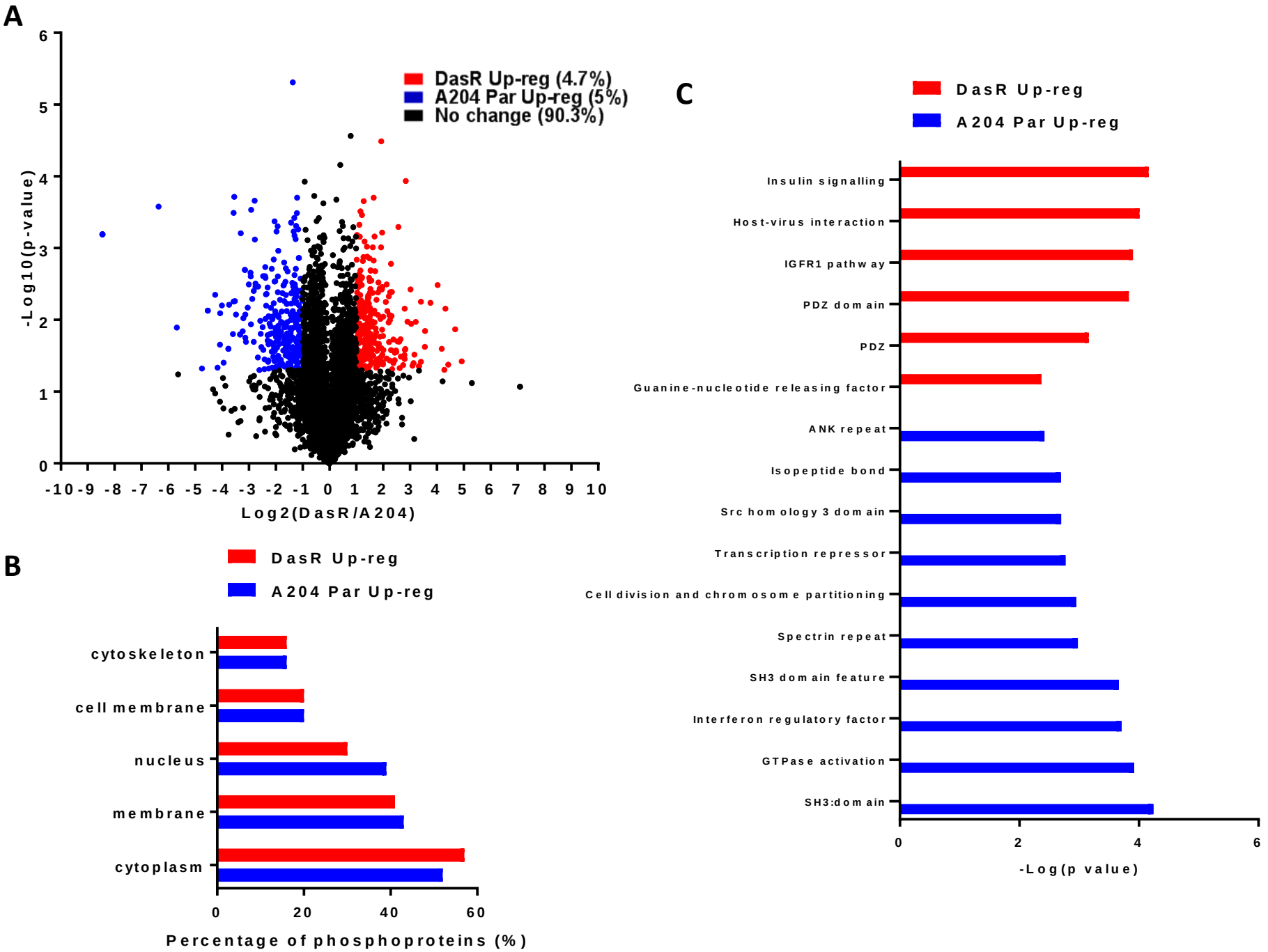
A
DasR Up-reg (4.7%)
A204 Par Up-reg (5%)
No change (90.3%)
-Log10(p-value)
Log2(DasR/A204)
B
DasR Up-reg
A204 Par Up-reg
cytoskeleton
cell membrane
nucleus
membrane
cytoplasm
Percentage of phosphoproteins (%)
C
DasR Up-reg
A204 Par Up-reg
Insulin signalling
Host-virus interaction
IGFR1 pathway
PDZ domain
PDZ
Guanine-nucleotide releasing factor
ANK repeat
Isopeptide bond
Src homology 3 domain
Transcription repressor
Cell division and chromosome partitioning
Spectrin repeat
SH3 domain feature
Interferon regulatory factor
GTPase activation
SH3:domain
-Log(p value)

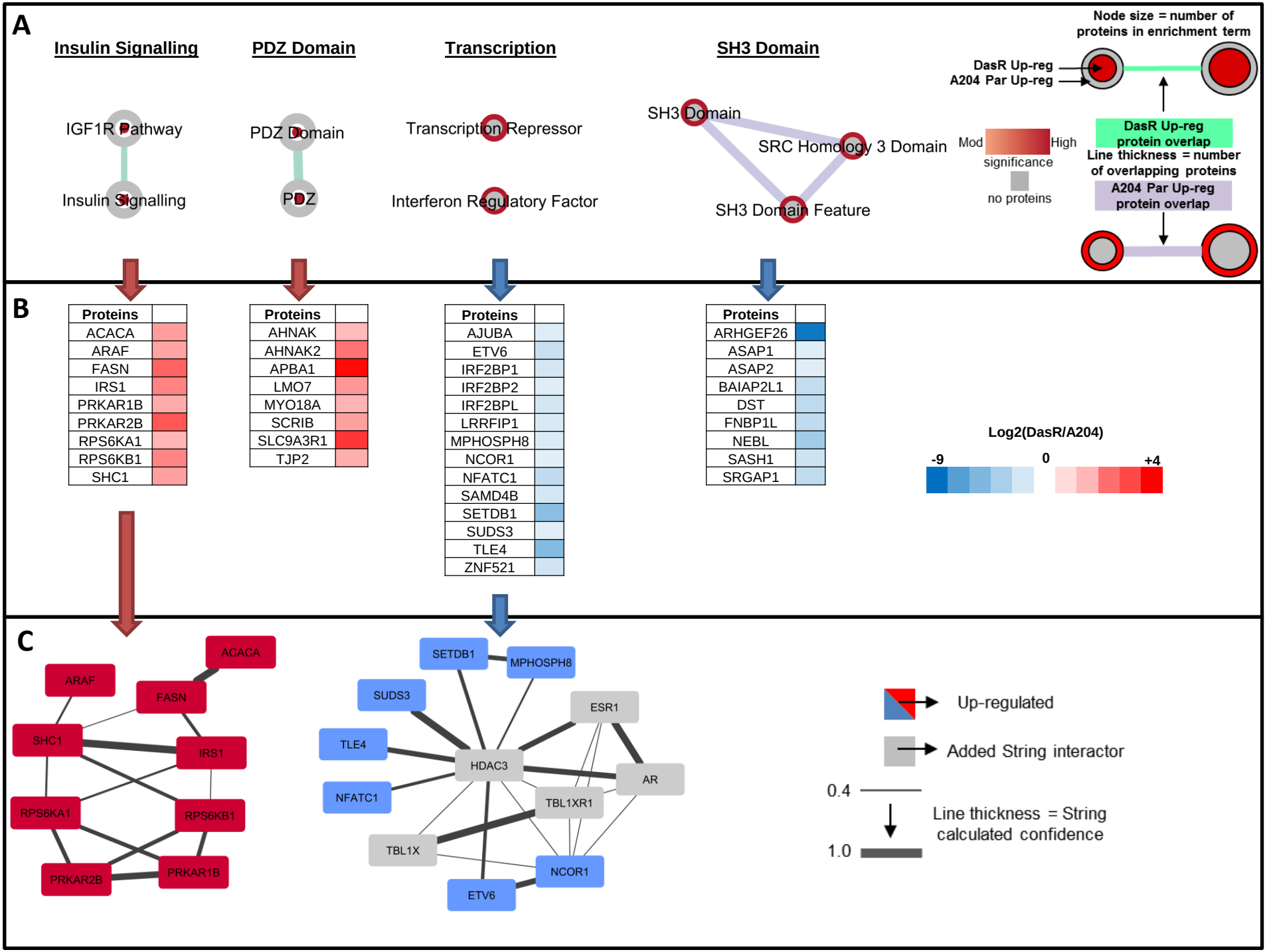
A
Insulin Signalling
PDZ Domain
Transcription
SH3 Domain
IGF1R Pathway
Insulin Signalling
PDZ Domain
PDZ
Transcription Repressor
Interferon Regulatory Factor
SH3 Domain
SRC Homology 3 Domain
SH3 Domain Feature
Node size = number of proteins in enrichment term
DasR Up-reg
A204 Par Up-reg
Mod
High
significance
no proteins
DasR Up-reg protein overlap
Line thickness = number of overlapping proteins
A204 Par Up-reg protein overlap
B
Proteins
ACACA
ARAF
FASN
IRS1
PRKAR1B
PRKAR2B
RPS6KA1
RPS6KB1
SHC1
Proteins
AHNAK
AHNAK2
APBA1
LMO7
MYO18A
SCRIB
SLC9A3R1
TJP2
Proteins
AJUBA
ETV6
IRF2BP1
IRF2BP2
IRF2BPL
LRRFIP1
MPHOSPH8
NCOR1
NFATC1
SAMD4B
SETDB1
SUDS3
TLE4
ZNF521
Proteins
ARHGEF26
ASAP1
ASAP2
BAIAP2L1
DST
FNBP1L
NEBL
SASH1
SRGAP1
Log2(DasR/A204)
-9
0
+4
C
ACACA
ARAF
FASN
SHC1
IRS1
RPS6KA1
RPS6KB1
PRKAR2B
PRKAR1B
SETDB1
MPHOSPH8
SUDS3
ESR1
TLE4
HDAC3
AR
NFATC1
TBL1XR1
TBL1X
NCOR1
ETV6
Up-regulated
Added String interactor
0.4
1.0
Line thickness = String calculated confidence

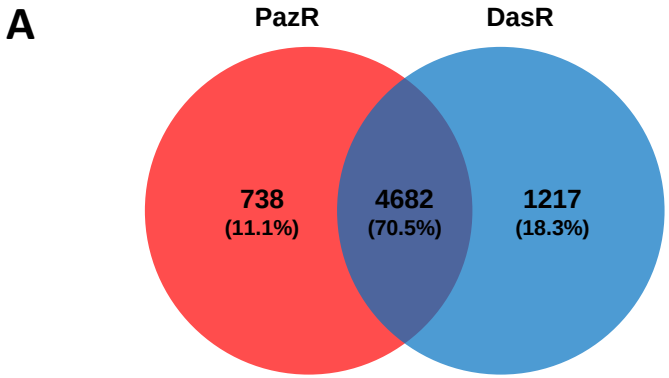

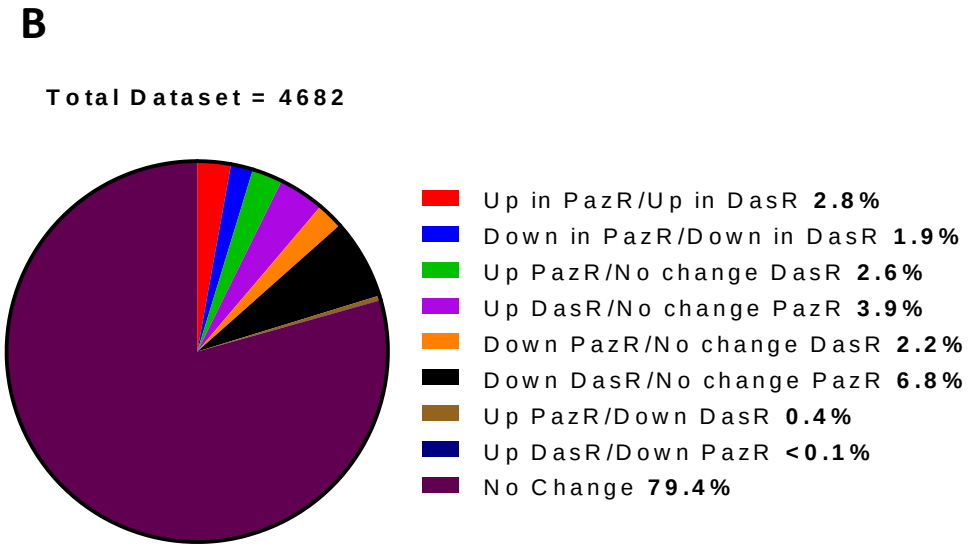

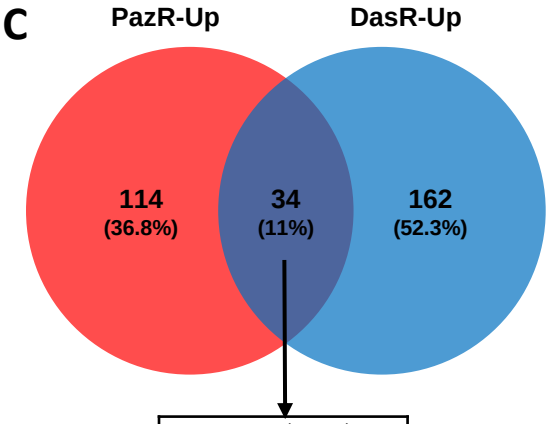

ARID1A (S1184)
CARHSP1 (S52)
DBN1 (S339)
DOS (S299)
DSP (S2222)
DSP (S2226)
DTX3L (S9)
EOMES (S107)
HEATR9 (T328)
IRS1 (S3)
LIMA1 (S15)
MAP1B (S1443)
MAP1B (S1792)
MAP1B (T1788)
MPST (S17)
MYPN (S759)
NF2 (S13)
PALM (S124)
PBXIP1 (S43)
PRKRA (S18)
PRRT3 (S431)
PTPN12 (S435)
RALGPS2 (S308)
SAMHD1 (T557)
SCRIB (T475)
SLC4A7 (S93)
TNKS1BP1 (S1620)
TNKS1BP1 (S1621)
TNKS1BP1 (S1666)
TNKS1BP1 (S429)
TNKS1BP1 (S672)
TNKS1BP1 (S836)
TNS3 (S776)
ZFP36L1 (S54)

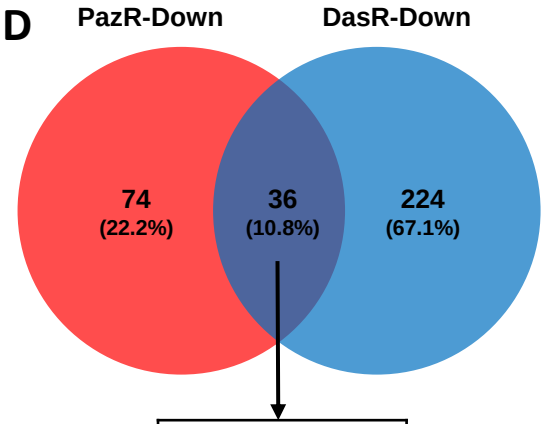

AKAP6 (S1073)
APPL1 (S401)
ARHGEF26 (S416)
ARHGEF26 (S419)
ARHGEF26 (S422)
ARHGEF26 (T417)
BAIAP2L1 (S414)
BICC1 (S803)
ETV6 (S22)
ETV6 (T18)
FN1 (S2006)
GNAS (S174)
GNAS (S230)
GNAS (S233)
HSPH1 (S765)
ITPKB (S174)
ITPKB (S176)
MAGED2 (S229)
MEF2A (S330)
MPHOSPH8 (S136)
MPHOSPH8 (S138)
NFATC1 (S220)
PDE8A (S385)
RCAN3;RCAN1 (S23)
RCAN3;RCAN1 (S27)
RIPK2 (S220)
RPS6KA3 (S369)
RPS6KA3 (S715)
RTN4 (T188)
SASH1 (S743)
SMAP2 (S139)
SOX6 (S358)
SYNE1 (S8234)
TBC1D4 (S570)
TBC1D4 (S666)
ZNF521 (S605)

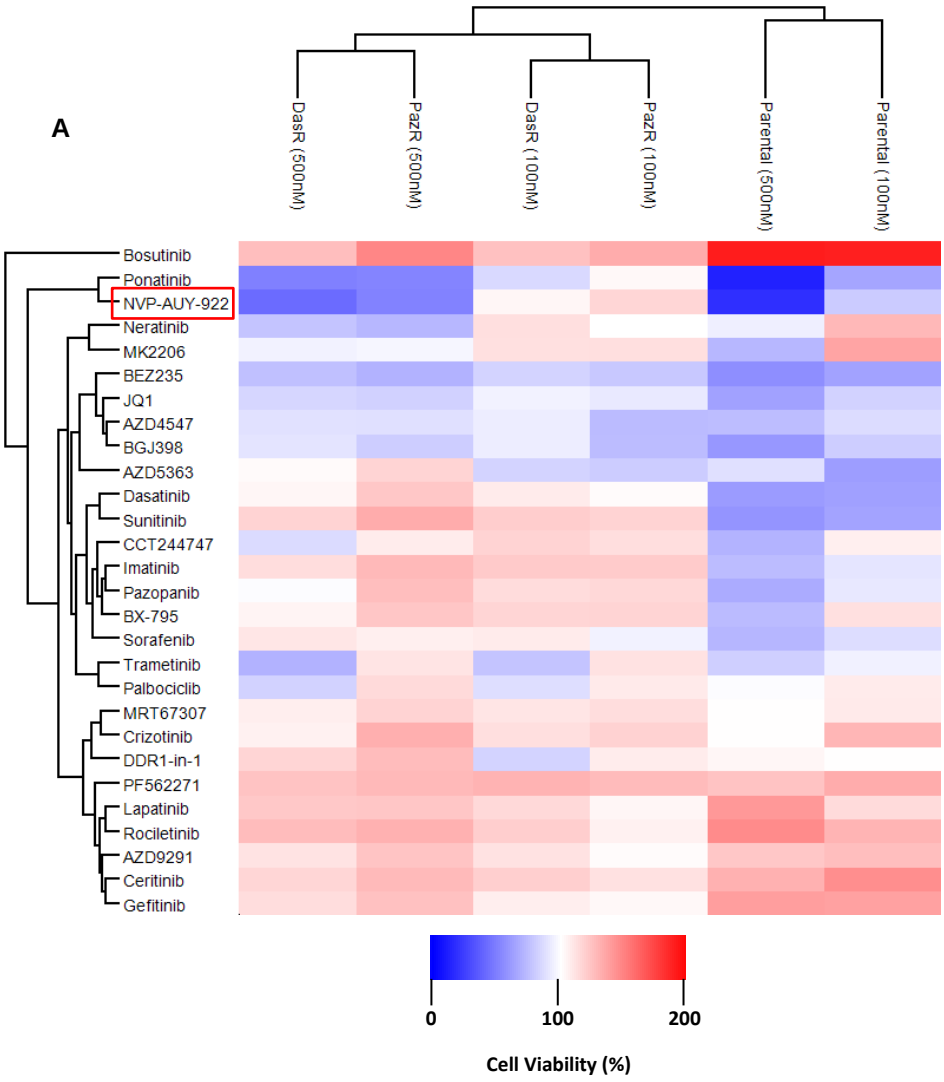
A
DasR (500nM)
PazR (500nM)
DasR (100nM)
PazR (100nM)
Parental (500nM)
Parental (100nM)
Bosutinib
Ponatinib
NVP-AUY-922
Neratinib
MK2206
BEZ235
JQ1
AZD4547
BGJ398
AZD5363
Dasatinib
Sunitinib
CCT244747
Imatinib
Pazopanib
BX-795
Sorafenib
Trametinib
Palbociclib
MRT67307
Crizotinib
DDR1-in-1
PF562271
Lapatinib
Rociletinib
AZD9291
Ceritinib
Gefitinib
0
100
200
Cell Viability (%)

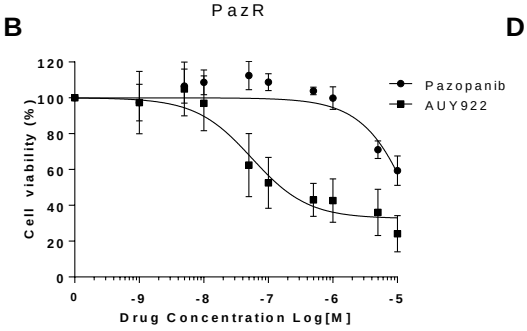
B
PazR
Pazopanib
AUY922
Cell viability (%)
Drug Concentration Log[M]

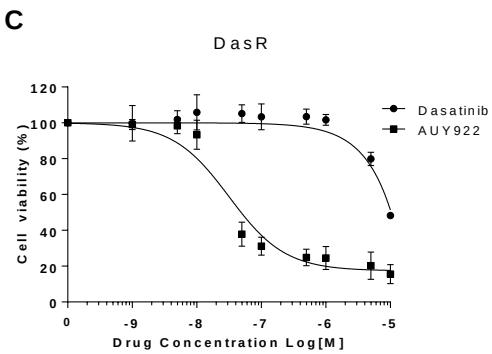
C
DasR
Dasatinib
AUY922
Cell viability (%)
Drug Concentration Log[M]

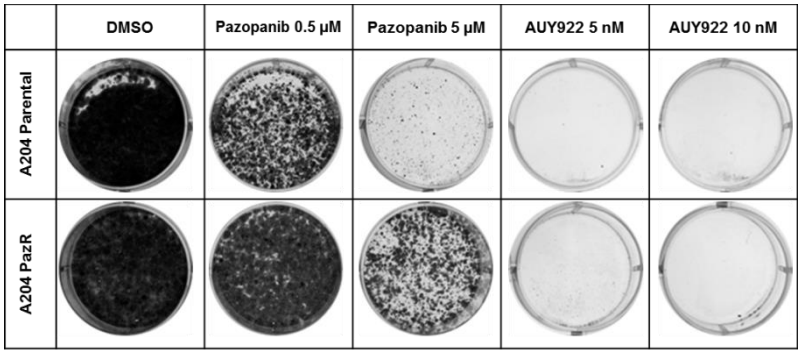
D
DMSO
Pazopanib 0.5 μM
Pazopanib 5 μM
AUY922 5 nM
AUY922 10 nM
A204 Parental
A204 PazR

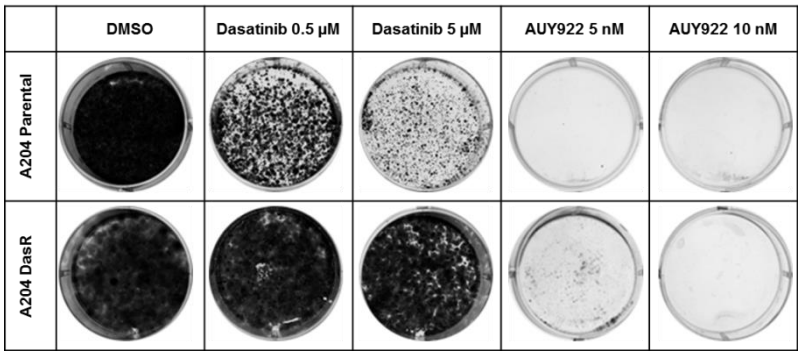
E
DMSO
Dasatinib 0.5 μM
Dasatinib 5 μM
AUY922 5 nM
AUY922 10 nM
A204 Parental
A204 DasR